
This copy is for your personal, non-commercial use only.

If you wish to distribute this article to others, you can order high-quality copies for your colleagues, clients, or customers by [clicking here](#).

Permission to republish or repurpose articles or portions of articles can be obtained by following the guidelines [here](#).

The following resources related to this article are available online at www.sciencemag.org (this information is current as of July 28, 2011):

Updated information and services, including high-resolution figures, can be found in the online version of this article at:

<http://www.sciencemag.org/content/333/6042/620.full.html>

Supporting Online Material can be found at:

<http://www.sciencemag.org/content/suppl/2011/07/27/333.6042.620.DC1.html>

This article **cites 28 articles**, 8 of which can be accessed free:

<http://www.sciencemag.org/content/333/6042/620.full.html#ref-list-1>

This article appears in the following **subject collections**:

Geochemistry, Geophysics

http://www.sciencemag.org/cgi/collection/geochem_phys

that may occur once farmers adjust their expectations of future climate. Examples of this would include expansion of crop area into cooler regions, switches to new varieties (17), or shifts toward earlier planting dates, although there is little evidence that the latter is happening beyond what is expected from historical responses to warm years (18). Moreover, the incentives to innovate have been limited in most of our sample period because prices have been low. On the other hand, our estimates may be overly optimistic because data limitations prevent us from explicitly modeling effects of extreme temperature or precipitation events within the growing season, which can have disproportionately large impacts on final yields (19). For example, although we captured the decline in growing-season total precipitation for wheat in India, there has also been a trend toward heavy rain events as an increased fraction of total rainfall, which is likely harmful to wheat yields (20).

Finally, we note that our study does not estimate the direct effect of elevated CO₂ on crop yields that are captured in the smooth time trends. Atmospheric CO₂ concentrations at Mauna Loa, Hawaii have increased from 339 ppm in 1980 to 386 ppm in 2008 (www.esrl.noaa.gov/gmd/ccgg/trends). Free-air CO₂ enrichment experiments for C₃ crops (i.e., wheat, rice, and soybean) show an average yield increase of 14% in 583 ppm CO₂ relative to 367 ppm CO₂ [i.e., 0.065% increase per ppm (21)]. This suggests that the 47 ppm increase since 1980 would have boosted yields by roughly 3%. Impacts of higher CO₂ on maize were likely much smaller because its C₄ photosynthetic pathway is unresponsive to elevated CO₂ (22). Thus, the net effects of higher CO₂ and climate change since 1980 have likely been slightly positive for rice and soybean, and negative for wheat and maize (Table 1).

The fact that climate impacts often exceed 10% of the rate of yield change indicates that climate changes are already exerting a considerable drag on yield growth. To further put this in perspective, we have calculated the impact of climate trends on global prices using recent estimates of price elasticities for global supply and demand of calories (23). The estimated changes in crop production excluding and including CO₂ fertilization (subtotal and total columns in Table 1, respectively) translate into average commodity price increases of 18.9% and 6.4% when we use the same bootstrap procedure as used in table 3 of (22).

Our study considers production of four major commodities at national scales. There are many important questions at subnational scales that our models cannot address, many important foods beyond the four modeled here, and many important factors other than food production that determine food security. Nonetheless, we contend that periodic assessments of how climate trends are affecting global food production can provide some useful insights for scientists and policy makers. This type of analysis should be accompanied by studies that evaluate the true pace and effectiveness of adaptation responses around

the world, particularly for wheat and maize. By identifying countries where the pace of climate change and associated yield pressures are especially fast, our study should facilitate these future analyses. Without successful adaptation, and given the persistent rise in demand for maize and wheat, the sizable yield setback from climate change is likely incurring large economic and health costs.

References and Notes

1. C. Rosenzweig, M. L. Parry, *Nature* **367**, 133 (1994).
2. J. Reilly et al., in *Impacts, Adaptations and Mitigation of Climate Change, Contribution of Working Group II to the Second Assessment Report of the Intergovernmental Panel on Climate Change*, R. T. Watson, M. C. Zinyowera, R. H. Moss, Eds. (Cambridge Univ. Press, London, 1996), pp. 427–467.
3. T. W. Hertel, M. B. Burke, D. B. Lobell, *Glob. Environ. Change* **20**, 577 (2010).
4. IPCC, in *Climate Change 2007: The Physical Science Basis. Contribution of Working Group I to the Fourth Assessment Report of the Intergovernmental Panel on Climate Change*, S. Solomon et al., Eds. (Cambridge Univ. Press, Cambridge, 2007); www.ipcc.ch/publications_and_data/ar4/wg1/en/spm.html.
5. D. B. Lobell, C. B. Field, *Environ. Res. Lett.* **2**, 004000 (2007).
6. See supporting material on Science Online.
7. K. G. Cassman, *Proc. Natl. Acad. Sci. U.S.A.* **96**, 5952 (1999).
8. J. Reilly, D. Schimmelpfennig, *Clim. Change* **45**, 253 (2000).
9. W. Schlenker, D. B. Lobell, *Environ. Res. Lett.* **5**, 014010 (2010).
10. D. B. Lobell, M. B. Burke, *Environ. Res. Lett.* **3**, 034007 (2008).
11. N. Brisson et al., *Field Crops Res.* **119**, 201 (2010).
12. J. K. Ladha et al., *Field Crops Res.* **81**, 159 (2003).
13. N. Kalra et al., *Curr. Sci.* **94**, 82 (2008).
14. J. R. Welch et al., *Proc. Natl. Acad. Sci. U.S.A.* **107**, 14562 (2010).
15. W. Easterling et al., in *Climate Change 2007: Impacts, Adaptation and Vulnerability. Contribution of Working Group II to the Fourth Assessment Report of the Intergovernmental Panel on Climate Change*, M. L. Parry et al., Eds. (Cambridge Univ. Press, Cambridge, 2007), pp. 273–313.
16. G. A. Meehl et al., in *Climate Change 2007: The Physical Science Basis. Contribution of Working Group I to the Fourth Assessment Report of the Intergovernmental Panel on Climate Change*, S. Solomon et al., Eds. (Cambridge Univ. Press, Cambridge, 2007), pp. 749–845.
17. Y. Liu, E. Wang, X. Yang, J. Wang, *Glob. Change Biol.* **16**, 2287 (2010).
18. N. Estrella, T. H. Sparks, A. Menzel, *Glob. Change Biol.* **13**, 1737 (2007).
19. W. Schlenker, M. J. Roberts, *Proc. Natl. Acad. Sci. U.S.A.* **106**, 15594 (2009).
20. B. N. Goswami, V. Venugopal, D. Sengupta, M. S. Madhusoodanan, P. K. Xavier, *Science* **314**, 1442 (2006).
21. E. A. Ainsworth, A. D. B. Leakey, D. R. Ort, S. P. Long, *New Phytol.* **179**, 5 (2008).
22. A. D. B. Leakey, *Proc. Biol. Sci.* **276**, 2333 (2009).
23. M. Roberts, W. Schlenker, *Identifying Supply and Demand Elasticities of Agricultural Commodities: Implications for the US Ethanol Mandate*, NBER Working Paper 15921 (National Bureau of Economic Research, Cambridge, 2010).

Acknowledgments: We thank five anonymous reviewers for helpful comments. Supported by a grant from the Rockefeller Foundation, NASA new investigator grant NNX08AV25G (D.B.L.), and NSF grant SES-0962625.

Supporting Online Material

www.sciencemag.org/cgi/content/full/science.1204531/DC1
Materials and Methods
Figs. S1 to S11
References

18 February 2011; accepted 22 April 2011
Published online 5 May 2011;
10.1126/science.1204531

Sr-Nd-Pb Isotope Evidence for Ice-Sheet Presence on Southern Greenland During the Last Interglacial

Elizabeth J. Colville,¹ Anders E. Carlson,^{1*} Brian L. Beard,¹ Robert G. Hatfield,² Joseph S. Stoner,² Alberto V. Reyes,¹ David J. Ullman¹

To ascertain the response of the southern Greenland Ice Sheet (GIS) to a boreal summer climate warmer than at present, we explored whether southern Greenland was deglaciated during the Last Interglacial (LIG), using the Sr-Nd-Pb isotope ratios of silt-sized sediment discharged from southern Greenland. Our isotope data indicate that no single southern Greenland geologic terrane was completely deglaciated during the LIG, similar to the Holocene. Differences in sediment sources during the LIG relative to the early Holocene denote, however, greater southern GIS retreat during the LIG. These results allow the evaluation of a suite of GIS models and are consistent with a GIS contribution of 1.6 to 2.2 meters to the ≥ 4 -meter LIG sea-level highstand, requiring a significant sea-level contribution from the Antarctic Ice Sheet.

The response of ice sheets to climate change is the largest source of uncertainty in predicting future sea-level rise (1). In the case of the Greenland Ice Sheet (GIS), observations of mass changes are restricted to the past few decades, providing limited context with which to assess present changes and future model predictions (1). An alternative approach for assessing the GIS response to climate change is to use the geologic record of the

GIS during earlier climate periods that were naturally warmer than the present in the boreal summer (2, 3), the season that affects GIS ablation.

¹Department of Geoscience, University of Wisconsin, Madison, WI 53706, USA. ²College of Oceanic and Atmospheric Sciences, Oregon State University, Corvallis, OR 97331, USA.

*To whom correspondence should be addressed. E-mail: acarlson@geology.wisc.edu

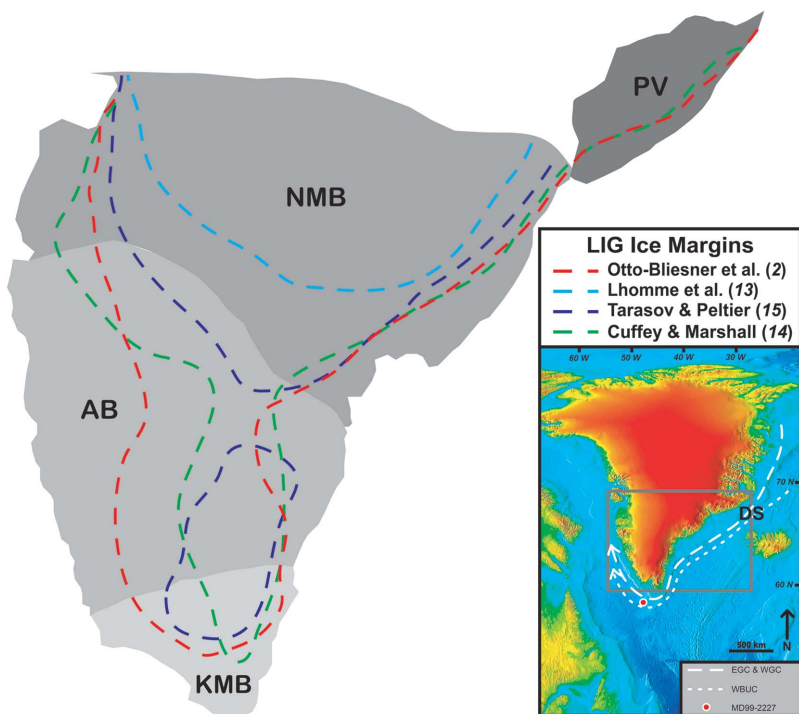


Fig. 1. Southern Greenland terrane map (20) with modeled LIG GIS margins (colored lines) (2, 13–15). All but one (13) of the depicted GIS extents agree with the isotopic record of GIS presence. Geologic terranes are indicated in gray scale. The inset shows the location of the map (box); ocean currents (white dashed lines; EGC, East Greenland Current; WGC, West Greenland Current); the Denmark Strait (DS); and cores MD99-2227 and HU90-013-013, collected ~300 m north of MD99-2227 (red dot).

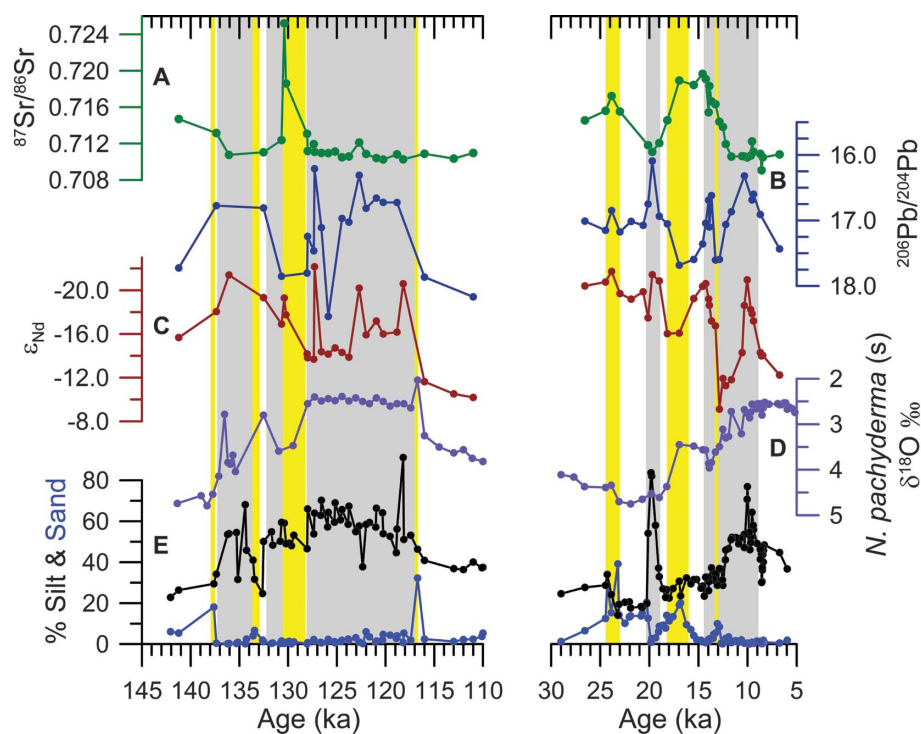


Fig. 2. MD99-2227 isotope and sediment records. (A) $^{87}\text{Sr}/^{86}\text{Sr}$ (green). (B) $^{206}\text{Pb}/^{204}\text{Pb}$ (blue). (C) Present-day ϵ_{Nd} values (red). (D) *Neogloboquadrina pachyderma* (sinistral) $\delta^{18}\text{O}$ (7) (purple). (E) Weight percent of silt (black) and sand (blue). Gray bars denote silt increases; yellow bars indicate IRD/Hudson Strait sediment (fig. S1).

The Last Interglacial [LIG, ~128 to 116 thousand years ago (ka)] is the most recent period with a boreal summer climate 0° to 5°C warmer than at present (2, 3). Global sea level was ≥ 4 m higher than at present and may have even exceeded ~ 8 m (4), indicating a smaller GIS and/or Antarctic Ice Sheet in addition to any ocean thermal expansion. Marine and ice-core records of GIS behavior suggest a smaller ice sheet (5–12) but provide only qualitative assessments of the magnitude of GIS retreat. Ice-sheet models also indicate a diminished GIS, predicting a 1.6- to 5.5-m contribution to the sea-level highstand (2, 13–16). Given this range in ice-sheet model predictions, the LIG sea-level highstand could be explained almost entirely by GIS retreat or require a significant fraction of sea-level rise from Antarctica. To better constrain the GIS response to a warmer climate and its LIG sea-level contribution, we investigated the presence or absence of ice on southern Greenland during the LIG through the determination of sediment sources discharged from southern Greenland during the last two glacial terminations (TI, ~20 to 6 ka; TII, ~138 to 128 ka) and the LIG, using the Sr-Nd-Pb isotopes of sediments in the Eirik Drift (Fig. 1). We focus on the southern GIS because ice-sheet models predict that this region is the most sensitive to LIG climate warming (2, 13–16).

Samples were collected from ocean core MD99-2227 (58.21°N, 48.37°W, 3460 m water depth), located on the Eirik Drift. The Eirik Drift monitors southern GIS behavior, receiving silt- and clay-sized sediment transported in the East and West Greenland Currents and Western Boundary Undercurrent (WBUC) (17, 18) (Fig. 1). We analyzed the silt-sized fraction for Sr-Nd-Pb isotope ratios rather than the clay-sized fraction (Fig. 2, A to C); the former is produced by glacial erosion (glacial flour) and probably supplied from Greenland, whereas the latter can be from far-traveled sources (17, 18). Details of the sampling rationale and procedures, sediment transport mechanisms to the Eirik Drift, analyses, and the core age model are provided in the supporting online material (19).

To avoid possible inputs from far-traveled ice-rafted debris (IRD) from icebergs or sea ice, intervals with abrupt increases in the percentage of sand were excluded from interpretations of Greenlandic source terranes (Fig. 2E). We also excluded Hudson Strait sediments discharged by the Laurentide Ice Sheet that were identified by abrupt increases in the percent of CaCO_3 and high Ca/Sr ratios, reflecting increased detrital carbonate deposition (fig. S1). The non-IRD and non-Hudson Strait silt-sized fraction of the Eirik Drift has four possible sources: WBUC- and Greenland Current-transported Paleogene volcanic (PV) detritus from East Greenland across the Denmark Strait to Iceland, and the three terranes that compose the southern Greenland Precambrian shield: the early Proterozoic Ketilidian Mobile Belt (KMB), the stable Archean Block (AB), and the Nagssugtoqidian Mobile Belt

(NMB) (17–20) (Fig. 1). Greenland sediments from north of the Denmark Strait (Fig. 1) could be transported to the Eirik Drift but have been identified only in the clay-sized fraction (18), and our isotope records indicate the absence of silt from north of the Denmark Strait in non-IRD layers.

The varying age and geologic histories of these four terranes result in each terrane having unique Sr-Nd-Pb isotope compositions (table S1) (19, 20). The PV is the youngest terrane and has the lowest $^{87}\text{Sr}/^{86}\text{Sr}$ ratios, highest Nd isotope (ϵ_{Nd}) values, and intermediate $^{206}\text{Pb}/^{204}\text{Pb}$ and $^{207}\text{Pb}/^{206}\text{Pb}$ ratios. The KMB is a Proterozoic terrane with moderate $^{87}\text{Sr}/^{86}\text{Sr}$ and $^{207}\text{Pb}/^{206}\text{Pb}$ ratios and ϵ_{Nd} values but very high $^{206}\text{Pb}/^{204}\text{Pb}$ ratios. The AB is the oldest terrane and has the highest $^{87}\text{Sr}/^{86}\text{Sr}$ and $^{207}\text{Pb}/^{206}\text{Pb}$ ratios and lowest ϵ_{Nd} values and $^{206}\text{Pb}/^{204}\text{Pb}$ ratios. The NMB is composed of Archean-age rocks that were deformed and metamorphosed during the Paleoproterozoic as well as some Paleoproterozoic-age crust, and has low ϵ_{Nd} values but relatively non-radiogenic $^{87}\text{Sr}/^{86}\text{Sr}$ ratios and $^{206}\text{Pb}/^{204}\text{Pb}$ ratios that are slightly greater and $^{207}\text{Pb}/^{206}\text{Pb}$ ratios that are slightly less than those of the AB.

During deglaciations, GIS retreat will expose subglacial sediment on the continental shelf and subsequently on land as an additional contribution to the sediment directly discharged from the ice margin (5–7, 18, 21). Upon reaching a new equilibrium state with climate, sediment discharge decreases in response to reduced ablation but does not cease (5–7, 18, 21). If, however, deglaciation leads to almost complete loss of ice from a given terrane (i.e., potentially small valley glaciers but no ice sheet/cap), then that terrane will not contribute a measurable amount of sediment to the Eirik Drift. Indeed, Greenland river suspended-load sediment concentrations are orders of magnitude lower for drainage basins that do not contain ice relative to glaciated basins (figs. S2 and S3). The Sr-Nd-Pb composition of Eirik Drift silt allows us to determine which terranes contained substantial amounts of melting glacial ice by identifying the source areas of sediment discharged from southern Greenland.

The MD99-2227 sedimentology record shows two periods of increased percentage of silt during TI at ~20.5 to 19 ka (~80% silt) and ~14.5 to 9 ka (~50% silt), with two intervening IRD events (Fig. 2E and fig. S1). (All percentages in the text are fractions of the total dry sediment weight.) During TII, the percentage of silt was elevated ~137 to 134 ka (~50% silt) and ~132 to 116 ka, peaking at ~126 to 123 ka, with three IRD events. Excluding IRD events, sand-sized particles are a small fraction of the total sediment (Fig. 2E), and clay-sized particles constitute much of the remaining sediment.

To determine the fraction of silt derived from Greenland, we used a simple four-component isotope mixing model between the southern Greenland Precambrian shield terranes and sediment transported from areas composed of PV (Fig. 1) (17–20). Our mixing model results suggest that

the Greenland Precambrian silt fraction of sediment increases from ~14 to 39% during the first TI silt increase and from ~14 to 21% during the second TI silt increase, with a temporary reduction to ~10% from ~12.5 to 11.7 ka (Fig. 3G). The reduction in the Precambrian Greenlandic silt fraction by ~7 ka suggests that the southern GIS had achieved equilibrium with Holocene climate (18, 19). During TII, the Greenland Precambrian silt fraction of the total sediment increases from ~9% at ~140 ka to ~32% by ~127 ka and remains elevated until decreasing back to ~9% by ~116 ka. The increases in percentage of silt therefore correspond to periods when southern Greenland-derived Precambrian detritus was a larger fraction of Eirik Drift sediment. Together with previous interpretations of GIS runoff events based on bulk-sediment Ti and Fe concentration (5) and magnetic grain size (6, 7), our results suggest a longer interval of enhanced ablation during TII

and the LIG relative to TI and the Holocene.

Greenlandic Precambrian silt source terranes changed between glacial periods, TI, TII, and the LIG (Fig. 3G and table S2). The Precambrian Greenlandic component of the low-silt intervals during glacial periods before TI and TII is derived primarily from the AB ($6 \pm 1\%$, $n = 6$ samples) and to a lesser extent from the NMB ($4 \pm 2\%$) and KMB ($2 \pm 1\%$), which is consistent with ice cover on all of southern Greenland but low sediment discharge. Periods of low silt after ~8 and 116 ka have slightly different Precambrian Greenlandic silt fractions (KMB = $3 \pm 1\%$; AB = $3 \pm 2\%$; NMB = $3 \pm 1\%$, $n = 6$ samples). PV silt increases during both terminations from glacial values of $13 \pm 3\%$ to interglacial values of $34 \pm 4\%$, reflecting intensification of the WBUC (Fig. 3F) (17, 18). The PV silt fraction remains elevated, however, at $29 \pm 3\%$ after ~8 and 116 ka, when the Precambrian Greenlandic silt fraction decreases (Fig. 3, F and

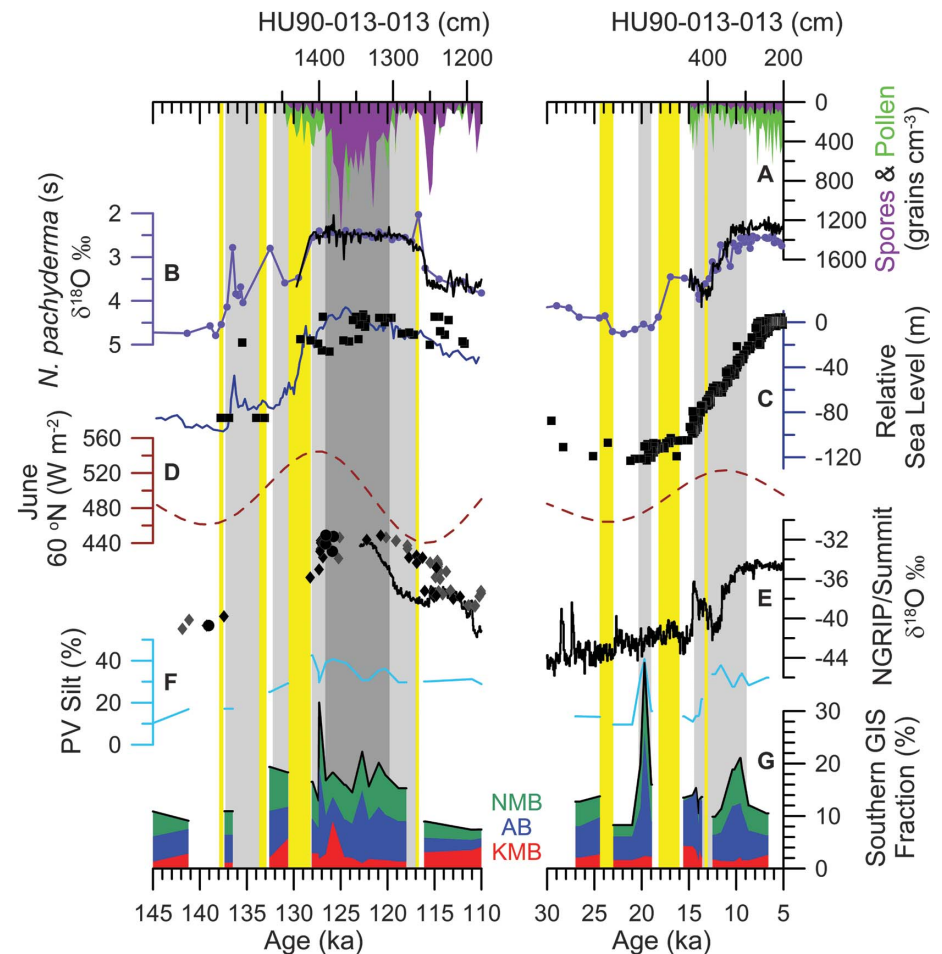


Fig. 3. Paleoclimate and southern GIS runoff records. (A) Abundance of pollen grains (green) and spores (orange) from HU90-013-013 (8). (B) *Neoglobobadrina pachyderma* (sinistral) $\delta^{18}\text{O}$ from MD99-2227 (purple) (7) and HU90-013-013 (black) (8) used to correlate the two cores. (C) Relative sea-level data (black) (22, 28, 29) and sea-level reconstruction (blue) (23). (D) June insolation at 60°N (red) (30). (E) North Greenland Ice Core Project (NGRIP) (step plot) (11) and Summit Greenland (12) $\delta^{18}\text{O}$ values; GRIP best estimates (gray diamonds), GISP2 best estimates (black diamonds), and GISP2 unique ages (black circles) are shown. (F) Fraction of total sediment composed of PV silt. (G) Fraction of total sediment composed of southern Precambrian Greenland silt (black line) and for the NMB (green), AB (blue), and KMB (red) terranes. Yellow and light gray bars are the same as in Fig. 2. The dark gray bar denotes the peak southern GIS retreat.

G), indicating that GIS runoff also controlled Precambrian Greenlandic sediment delivery to the Eirik Drift in addition to the WBUC.

The first TI silt increase is largely derived from the AB and NMB ($23 \pm 6\%$ AB+NMB, $n = 3$ samples), whereas the second TI silt increase initially has a larger fraction derived from the KMB ($4 \pm 1\%$, $n = 4$ samples), with the latter part coming mainly from the AB ($10 \pm 1\%$, $n = 3$ samples) and NMB ($8 \pm 1\%$) (Fig. 3G). All three isotope systems are measured only on silt from the beginning of the first TII silt increase, which suggests AB and NMB sources ($10 \pm 3\%$ AB+NMB, $n = 1$ sample). The second silt increase of TII, which also spans the LIG, shows greater variability in the isotopic ratios (Fig. 2, A to C). Between ~ 132 and 126 ka, the KMB silt component periodically increases from $2 \pm 1\%$ up to $9 \pm 2\%$. The AB and NMB silt fractions remain relatively constant, with a notable peak at ~ 127 ka, when $30 \pm 8\%$ of the sediment is silt from the AB and NMB. After ~ 126 ka, the KMB silt portion reduces to $2 \pm 1\%$ ($n = 7$ samples) for the remainder of the LIG, whereas the AB and NMB fractions increase to $9 \pm 3\%$ and $7 \pm 1\%$, respectively, until the end of the LIG.

Our results indicate that the AB, NMB, and KMB terranes contributed sediment to the Eirik Drift throughout the LIG (Fig. 3G), signifying that, as in TI and the Holocene (15, 19), the southern GIS did not completely deglaciate any one terrane. However, the larger KMB silt component of the total sediment during the first half of the LIG implies a longer period of ice adjustment to equilibrium on the KMB terrane and greater ice retreat relative to the Holocene. The elevated fraction of AB and NMB silt throughout the LIG suggests that ice on these terranes may not have reached equilibrium, with continued retreat through the LIG until North Atlantic cooling into the next ice age (Fig. 3). Indeed, between ~ 127 and 120 ka, Greenlandic pollen and spores reach maximum concentrations in Eirik Drift sediment, implying the greatest expansion of vegetation on Greenland and the minimum in ice extent (8) (Fig. 3A). Given LIG age-model uncertainties (19), this interval of greatest southern GIS retreat corresponds to the peak in boreal summer insolation (Fig. 3D), highest Summit Greenland $\delta^{18}\text{O}$ (12) (Fig. 3E), and maximum sea level of ≥ 4 m (Fig. 3C) (3, 4, 22, 23).

The radiogenic isotope data allow us to differentiate between five existing GIS modeled LIG ice volumes (2, 13–16). Ice-sheet models that predict a GIS extent with ice still remaining on all three southern Greenland terranes, consistent with our data and some ice-core interpretations (10, 11), indicate a GIS sea-level contribution of 1.6 to 2.2 m to the ≥ 4 -m sea-level highstand [the maximum extents predicted by (2, 14, 15)] (Fig. 1). Ice-sheet models that suggest larger GIS sea-level contributions have at least one southern Greenland terrane deglaciated [the minimum extents of (2, 14, 15) and extents of (13, 16)], which is inconsistent with our data.

These results strongly suggest that the GIS contributed a significant component of the LIG sea-level highstand, although at the lower end of previous estimates (2, 3, 13–16). A larger GIS contribution to sea level could be explained by greater retreat of its northern margin outside our region of study, but Greenland ice-core $\delta^{18}\text{O}$ and total gas records suggest only small changes in north Greenland ice thickness between the LIG and the present, arguing against a large contribution from this sector (11, 12). Additional LIG sea-level contributions could have come from the disappearance of Arctic-Icelandic glaciers and ice caps, adding 0.3 to 0.4 m of sea-level equivalent volume (2) and 0.04 to 0.4 m of ocean thermal expansion (1) from 0.2° to 0.6°C of global warming relative to the present (24, 25). Together, these contributions indicate that the Antarctic Ice Sheet must have provided ≥ 1.0 m of sea-level equivalent volume to the LIG highstand, which is in agreement with ice-sheet (16, 26) and earth (4) models, and confirms that it is also sensitive to relatively small changes in radiative forcing (3, 4, 26, 27).

References and Notes

- G. A. Meehl *et al.*, in *The Physical Basis of Climate Change: Contribution of Working Group 1 to the Fourth Assessment Report of the IPCC* (Cambridge Univ. Press, Cambridge, 2007).
- B. L. Otto-Bliesner, S. J. Marshall, J. T. Overpeck, G. H. Miller, A. Hu, *Science* **311**, 1751 (2006).
- J. T. Overpeck *et al.*, *Science* **311**, 1747 (2006).
- R. E. Kopp, F. J. Simons, J. X. Mitrovica, A. C. Maloof, M. Oppenheimer, *Nature* **462**, 863 (2009).
- A. E. Carlson, J. S. Stoner, J. P. Donnelly, C. Hillaire-Marcel, *Geology* **36**, 4 (2008).
- J. S. Stoner, J. E. T. Channell, C. Hillaire-Marcel, *Geology* **23**, 241 (1995).
- H. F. Evans *et al.*, *Geochem. Geophys. Geosyst.* **8**, Q11007 (2007).
- A. de Vernal, C. Hillaire-Marcel, *Science* **320**, 1622 (2008).

- R. M. Koerner, D. A. Fisher, *Ann. Glaciol.* **35**, 19 (2002).
- E. Willerslev *et al.*, *Science* **317**, 111 (2007).
- North Greenland Ice Core Project members, *Nature* **431**, 147 (2004).
- M. Suwa *et al.*, *J. Geophys. Res.* **111**, D02101 (2006).
- N. Lhomme, G. K. C. Clarke, S. J. Marshall, *Quat. Sci. Rev.* **24**, 173 (2005).
- K. M. Cuffey, S. J. Marshall, *Nature* **404**, 591 (2000).
- L. Tarasov, W. R. Peltier, *J. Geophys. Res.* **108**, 2143 (2003).
- P. Huybrechts, *Quat. Sci. Rev.* **21**, 203 (2002).
- C. Innocent, N. Fagel, R. K. Stevenson, C. Hillaire-Marcel, *Earth Planet. Sci. Lett.* **146**, 607 (1997).
- N. Fagel *et al.*, *Paleoceanography* **19**, PA3002 (2004).
- See supporting material on Science Online.
- P. R. Dawes, *Geol. Surv. Denmark Greenland Bull.* **17**, 57 (2009).
- B. Hallet, L. Hunter, J. Bogen, *Global Planet. Change* **12**, 213 (1996).
- W. G. Thompson, S. L. Goldstein, *Science* **308**, 401 (2005).
- E. J. Rohling *et al.*, *Nat. Geosci.* **2**, 500 (2009).
- Q. Z. Yin, A. Berger, *Nat. Geosci.* **3**, 243 (2010).
- G. Schurgers *et al.*, *Clim. Past* **2**, 205 (2006).
- D. Pollard, R. M. DeConto, *Nature* **458**, 329 (2009).
- J. H. Mercer, *Nature* **271**, 321 (1978).
- A. L. Thomas *et al.*, *Science* **324**, 1186 (2009).
- P. U. Clark *et al.*, *Science* **325**, 710 (2009).
- A. Berger, M. F. Loutre, *Quat. Sci. Rev.* **10**, 297 (1991).

Acknowledgments: J. Briner and the Greenland Institute of Natural Resources kindly provided several stream and iceberg silt samples. E. Obbink, K. Winsor, B. Welke, S. Strano, and A. Leaf provided assistance in the field and laboratory. D. Kelly and C. Hillaire-Marcel supplied comments on this research and manuscript. A. de Vernal provided her pollen records. This research was supported by the Geological Society of America and American Association of Petroleum Geologists (E.J.C.), University of Wisconsin–Madison startup funds (A.E.C.), and the Arctic Natural Sciences Division of NSF, Arctic Natural Sciences grants 0902571 (A.E.C. and B.L.B.) and 0902751 (J.S.S.).

Supporting Online Material

www.sciencemag.org/cgi/content/full/333/6042/620/DC1
Materials and Methods
Figs. S1 to S5
Tables S1 to S5
References

22 February 2011; accepted 27 May 2011
10.1126/science.1204673

Tenfold Population Increase in Western Europe at the Neandertal-to-Modern Human Transition

Paul Mellars* and Jennifer C. French

European Neandertals were replaced by modern human populations from Africa $\sim 40,000$ years ago. Archaeological evidence from the best-documented region of Europe shows that during this replacement human populations increased by one order of magnitude, suggesting that numerical supremacy alone may have been a critical factor in facilitating this replacement.

Neandertal populations were replaced by anatomically and genetically modern human populations across Europe, between $\sim 45,000$ and $35,000$ years before the present (yr B.P.). The reasons for the success of modern humans and the associated issues of Neandertal extinction have been widely debated (1–11). Any process of population replacement and extinc-

tion reduces ultimately to a question of numbers: the increase of the incoming population versus the decline of the resident population (12, 13).

Department of Archaeology, Cambridge University, Cambridge CB2 3DZ, UK.

*To whom correspondence should be addressed. E-mail: pam59@cam.ac.uk